International Journal of ChemTech Research
CODEN (USA): IJCRGG ISSN: 0974-4290
Vol.7, No.3, pp 1644-1650, 2014-2015

ICONN 2015 [4th - 6th Feb 2015]
International Conference on Nanoscience and Nanotechnology-2015
SRM University, Chennai, India

Raman and Photoluminescence Studies of Ag and Fe-doped ZnO Nanoparticles

M. Silambarasan[1]*, S. Saravanan[1], T. Soga[2]

[1]Centre for Photonics and Nanotechnology, Sona College of Technology, Salem -5, Tamil Nadu, India
[2]Department of Frontier Materials, Nagoya Institute of Technology, Nagoya 466-8555, Japan

Abstract: In this paper, we report a comparative study of Raman and photoluminescence (PL) studies of Ag and Fe-doped ZnO nanoparticles synthesized by simple solution combustion method. The powder X-ray diffraction (XRD) pattern indicates that the Ag and Fe-doped ZnO samples exhibit primary and secondary phases. The both primary phase indicates the hexagonal wurtzite structure with the average crystalline size of around 25-50 nm. The Raman scattering of the pure ZnO shows the first and second orders of polar and non-polar modes which are the characteristic bonds of the wurtzite ZnO. The Raman spectra of the Ag and Fe-doped ZnO nanoparticles confirm considerable effect on the polar and non-polar branches. Room temperature PL results indicate the near band edge related emission and the results are related to several intrinsic defects in the Ag and Fe-doped ZnO nanoparticles. The PL results show the enhanced optoelectronic properties, in particular, the oxygen vacancies are responsible for the long life time of the carriers.
Keywords: Raman and Photoluminescence Studies, Ag, Fe-doped ZnO Nanoparticles.

Introduction:

Zinc Oxide (ZnO) nanomaterials have played a very important role among all other metal oxides for many applications due to its unique and interesting properties, such as electrical, optical, chemical and eco-friendly[1-3]. The ZnO is a potential candidate for the optoelectronics, photonics and piezoelectric applications due to its wide band gap (3.37eV) and large exciton binding energy (60 meV) in room temperature. The ZnO has greatest variety of nanostructures. The ZnO is one of the most significant materials for various potential applications such as photo detectors, laser diode, sensors, flexible and polymer based solar cells and an electrode in dye sensitized solar cells. Recently, many research groups are working for the development of ZnO nanostructures based white light emitting diode (LED) as an alternative source to enabled bright and energy-saving light sources[4-6].

The ZnO has greatest variety of morphologies such as, nanorods, nanowires, nanotubes, pyramidal, spheres, whiskers, flowers and so on. Many methods have been developed to prepare the ZnO nanoparticles such as, wet chemical synthesis, sol-gel technique, gas-phase reactions, template assisted growth, chemical precipitation, ball milling, organometallic synthesis, spray pyrolysis, hydrothermal method and mechano

chemical synthesis, etc[1,4,7-10]. Transition metal doped ZnO systems are actively promising candidate for spintronics and photonics applications due to their unique properties[11-13]. Raman spectroscopy is a nondestructive characterization technique on vibrational properties of ZnO nanostructures. The optical phonon confinement in the ZnO nanostructures has lead to the interesting changes in its vibrational spectra than the bulk ZnO. Moreover, the Raman spectroscopy is a versatile technique to study the doping agent incorporation and impurity induced modes of ZnO nanoparticles doped with metals[14]. The optical properties of ZnO can be improved by incorporating various ions in the crystal lattice[15]. The PL emission spectroscopy is a traditional technique in order to determine optical properties and internal defects of metal doped ZnO nanostructures[16,17].

In this paper, we are discussed a comparative study of Raman and PL studies of Ag and Fe-doped ZnO nanoparticles which are synthesize by simple solution combustion method.

Experimental Methods:

The synthesis methods of ZnO nanoparticles have been reported already[18,19]. Typical synthesis, 0.05 M of zinc acetate dihydrate is dissolved in 100 ml of mixed solvents as of ethanol and ethylene glycol (EG) with the volume ratio of 60/40 ml, respectively. Subsequently, different millimoles of silver nitrate/ ferrous sulfate are mixed into the above solution under constant magnetic stirring. The solution is transferred into a spirit lamp with an absorbent cotton lamp wick and followed by the spirit lamp is fired. Later the lamp wick is extinguished; the samples are continually dispersed into distilled water to wash and remove the impurity by ultrasonic process. Finally, the samples are dried out in hot air oven.

The crystalline properties of the prepared samples are studied by powder XRD. The XRD of the samples are carried out by a Rigaku Rint 2100 with Cu Kα radiation (λ = 0.15 nm) at the scanning rate of 0.02˚/s for the 2θ value of 20 to 70˚. Surface morphology of the prepared nanoparticles has investigated by field emission-scanning electron microscopy (FE-SEM) which is analyzed through Quanta-200F SEM. The vibrational properties of the synthesized ZnO nanoparticles are investigated by Raman spectra. The high resolution Raman spectra collected at room-temperature by Jobin-Yvon LabRAM-HR800 instrument with an Ar^+ laser line (λ = 514 nm) as the excitation source, the size of the laser spot was 1 μm in diameter and the laser power on the sample was 30 mW with the thermo electrically cooled charge coupled device (CCD) detector. The Raman spectral resolution was 0.3 cm^{-1}. All Raman spectra are recorded in the region of 50–1200 cm^{-1} at the backscattering geometry. The room temperature PL spectra are recorded to study the optical characterization of the ZnO nanoparticles using a Horiba Jobin spectrofluorometer with the source of xenon lamp (450 W) at excitation wavelength of 325 nm.

Result and Discussion:

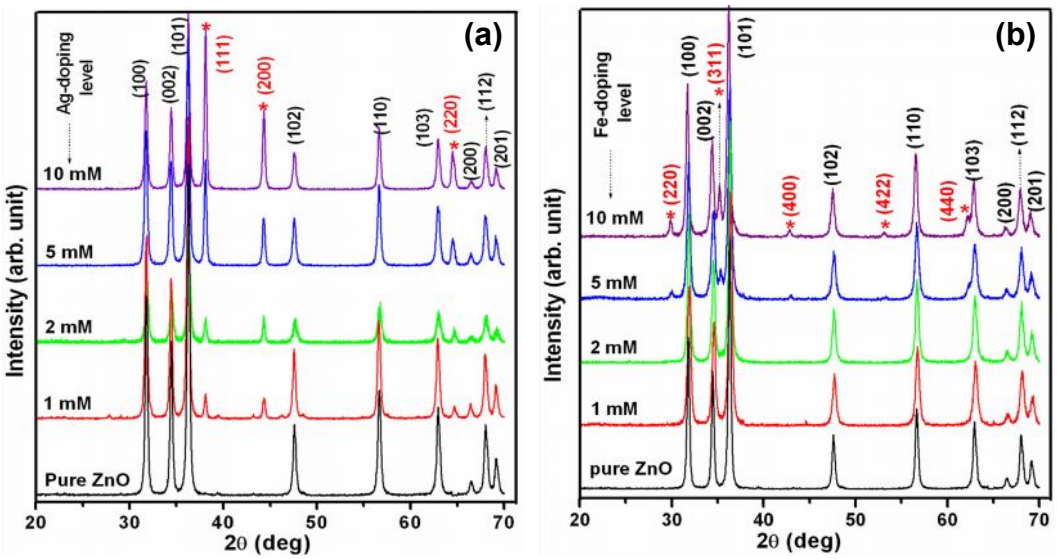

Figure 1: Powder XRD of (a) pure with Ag-doped ZnO nanoparticles and (b) pure with Fe-doped ZnO nanoparticles for 0.05 M zinc precursor with different millimole of respective doping agent.

Figures 1(a) and 1(b) show the powder XRD of pure, Ag-doped and Fe-doped ZnO nanoparticles for various millimoles of Ag and Fe doping, respectively. The Ag and Fe-doped samples reveal primary and secondary phases. The primary phase is well matched with JCPDS No. 05-0664 and all diffraction lines are assigned well to the hexagonal phase of wurtzite structure of ZnO. The secondary phase of Ag-doped samples exposes some additional diffraction peaks at 2θ = 38, 44, and 64° (marked by asterisks) associated with JCPDS No. 04-0783 which indicates the face centered cubic (FCC) phase of metallic Ag[19], whereas the secondary phase of Fe-doped ZnO samples show some additional diffraction peaks at 2θ = 29°, 35°, 42°, 53° and 62° (marked by asterisks) associated with JCPDS No: 89-0951[20] which is assigned to the FCC phase of magnetite iron oxide (Fe_3O_4). When increasing the doping concentration of Ag and Fe, the intensity of the secondary phase peaks is increased. The crystalline sizes are varied from 25 to 50 nm for both Ag and Fe-doped ZnO samples. The surface morphology of pure, Ag and Fe-doped samples are obtained from FE-SEM images as shown in figure 2(a) – 2(c), respectively, and from the figure, the particles are aggregated to each other.

The Raman spectrum is an essential and versatile diagnostic tool in order to study the crystallization, structural disorder and defects in micro and nanostructures. The vibrational properties of the synthesized ZnO nanoparticles are investigated by Raman spectra. The ZnO nanoparticles with hexagonal wurtzite structure fit into the space group of *P*63*mc*. For the perfect ZnO crystal, only the optical phonons at Γ point of the Brillouin zone are involved in first-order Raman scattering. According to the group theory, optical modes should exist in a wurtzite ZnO are given in equation (1).

$$\Gamma_{opt} = A_1 + 2B_2 + E_1 + 2E_2 \qquad \text{---------- (1)}$$

Where, both A_1 and E_1 modes are two polar branches, which is spilt into longitudinal optical (LO) and transversal optical (TO) components with different frequencies due to macroscopic electric fields associated with the LO phonons. The A_1, E_1, and E_2 modes are first order Raman-active modes.

According to the Raman selection rule, the B_1 modes are generally inactive in Raman spectra and are called silent modes[21]. Figure 3 shows the Raman spectra of pure ZnO nanoparticles. The basic phonon modes of hexagonal ZnO has been obtained at 100, 385, 440 and 585 cm^{-1}, which represents to the E_{2L}, A_1(TO), E_{2H} and A_1(LO)/E1(LO), respectively. The second order phonon mode has presented at about 150 cm^{-1} that is assigned to $2E_{2L}$. The multi phonon scattering modes are presented at 331, 508, 664 and 1065 cm^{-1} which are assigned to the $3E_{2H}$-E_{2L}, E_1(TO)+E_2L, 2(E_{2H}-E_{2L}) and A_1(TO)+E_1(TO)+E_{2L}, respectively. Also, the acoustic combination of A_1 and E_2 are observed around 1101 cm^{-1}.

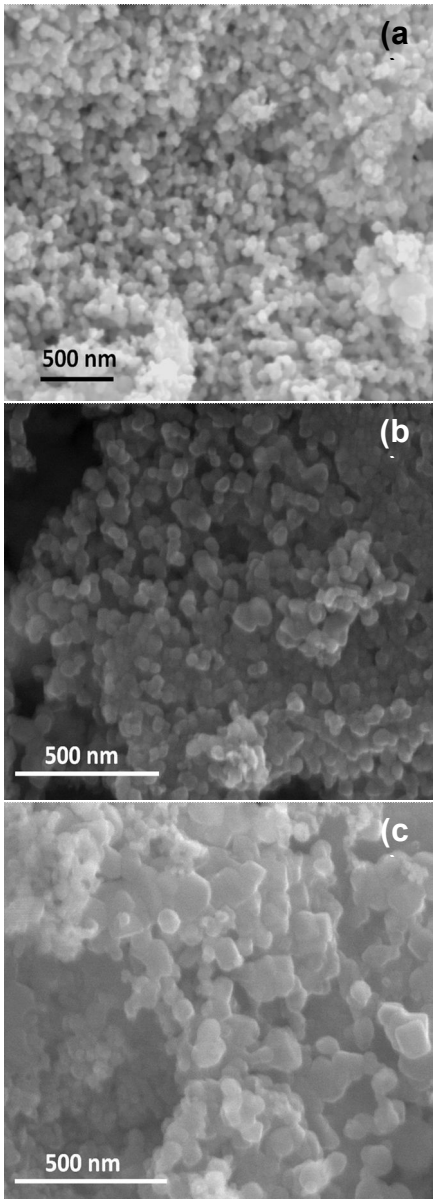

Figure 2: FE-SEM images of (a) pure ZnO, (b) Ag-doped ZnO and (c) Fe-doped ZnO nanoparticles.

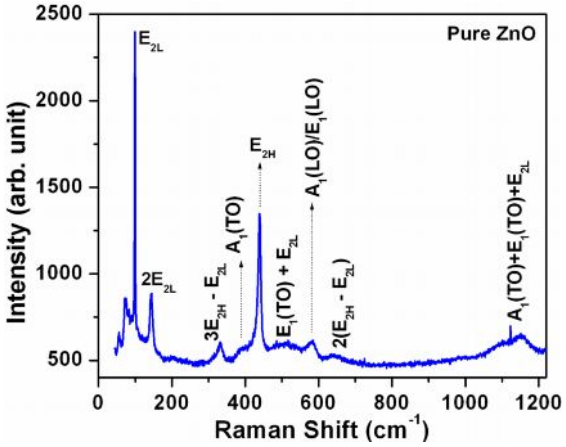

Figure 3: Micro Raman spectra of pure ZnO nanoparticles for 0.05 M zinc precursor.

Figure 4 shows the Raman spectra of ZnO nanoparticles with Ag and Fe-doping of 2 and 10 mM, respectively. The polar and non polar modes are significantly changed with respect to the doping agent (both

Ag and Fe) on ZnO matrix. E_{2H} mode involves the oxygen motion, sensitive to internal stress and is characteristic of hexagonal wurtzite structure of ZnO nanostructures. The E_{2H} mode has a huge reduction in the intensity of Ag-doped samples due to breakdown of translational crystal symmetry by the incorporation of impurities as well as defects, while the E_{2H} mode has been steadily decreased and broadened when increase the Fe-doping concentrations. Also, the polar mode of $A_1(LO)/E_1(LO)$ at around 570 cm^{-1} has been presented for both Ag and Fe-doping and this peak is broadened as well as shifted to lower energy. All the shifting and broadening of phonon modes are represented that the scattering contributions have obtained outside the Brillouin zone centre. The $A_1(LO)/E_1(LO)$ phonon mode is usually represented to the defect complexes of zinc interstitial and oxygen vacancy in ZnO lattice. The intensity of Ag-doped ZnO Raman peaks increases enormously due to the incorporation of Ag ions the ZnO nanoparticles. Also, the results further confirm that ZnO nanoparticles contained crystallization with few defects due to Ag ions. In the Fe-doped samples, the broad peak observed at around 665 cm^{-1} is due to Fe-ions incorporated into ZnO matrix.

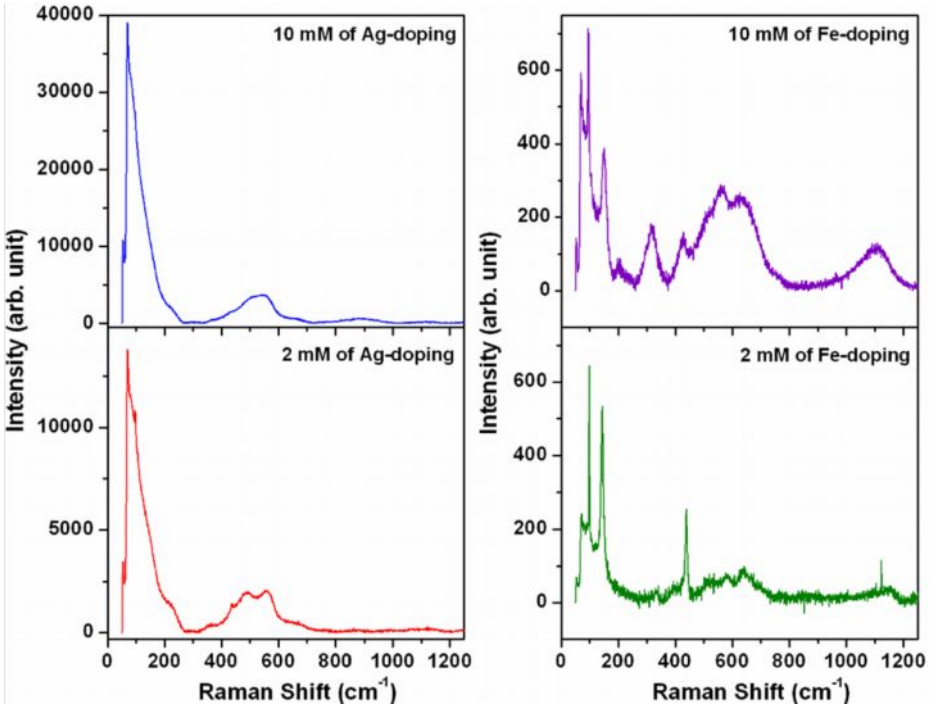

Figure 4: Micro Raman spectra of Ag and Fe-doped ZnO nanoparticles with different millimole of respective doping agent.

It might be represented as Fe_3O_4 and related to intrinsic lattice defects, which become activated as vibrating complex. Also, the results of Ag and Fe-doped samples are coincided with XRD results of secondary phase formations.

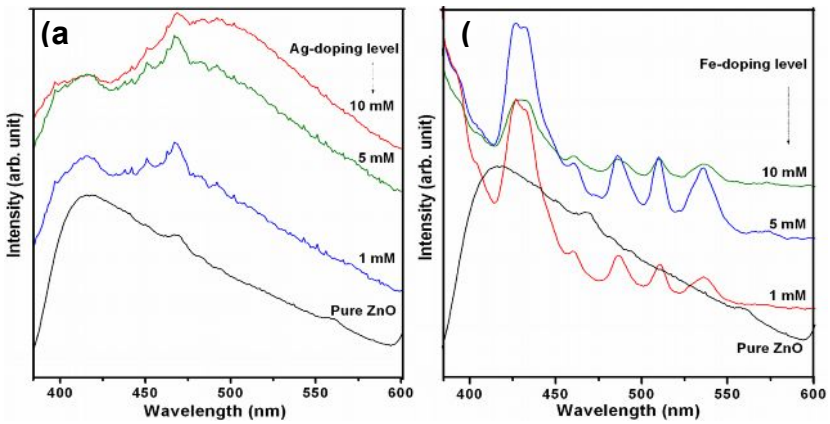

Figure 5: Room temperature PL spectra of (a) pure with Ag-doped and (b) pure with Fe-doped ZnO nanoparticles for 0.05 M zinc precursor with different millimole of corresponding doping agent.

The PL spectra of pure with various millimoles of Ag and Fe-doping are shown in figure 5(a) and 5(b), respectively. The pure ZnO nanoparticles show the PL emission peak at 415 nm (2.98 eV). The strong blue emission represents the exciton recombination which is related to near-band edge (NBE) emission of ZnO. Also, the shoulder peaks of blue (around 450 and 467 nm), blue-green (494 nm), and green (558 nm) emission are obtained on the broad PL spectrum. In general, the visible emissions are related to several intrinsic defects in ZnO NPs, which contains Zn vacancies (V_{Zn}), oxygen vacancy (V_O), zinc interstitial (Zn_i), interstitial O (O_i), substitution of O at Zn position (O_{Zn}) and complex of V_O and Zn_i (V_OZn_i)[22]. The NBE related emissions of the Ag-doped ZnO nanoparticles obtained in blue region has similar trend as obtained in pure ZnO nanoparticles, whereas the Fe-doped samples show blue shift into UV region due to Burstein-Moss effect. Due to the Burstein-Moss effect in metal doped ZnO, the Fermi level shifted into the conduction band (C_B)[23]. It can be represented that the absorption transition changed the Fermi level within the C_B from the bottom of the C_B[24]. Therefore, the changes in transition levels lead to the energy gap broadening and result in the blue shift. The blue shift of the emission in UV region is changed with respect to the doping agent.

In the Ag-doped ZnO samples (Fig-5a), the shoulder peaks of blue and green emissions (450 – 560 nm) are increased than the pure samples on the broad PL spectrum. In the Fe-doped samples (Fig-5b), the strong blue emission at around 430 nm is greatly activated when compared with Ag-doped and pure ZnO samples. This strong blue emission might be due to two defect levels, either transition from bottom of the C_B to O_i level or transition from Zn_i to V_B[25]. Ag-doped ZnO samples (Fig-5a) show that the peak at around 475 nm has more dominant and broadening for all the doped samples compared with pure ZnO. The blue and weak blue-green (450 - 495 nm) emissions may be due to surface defects in the ZnO nanoparticles. The weak green (around 550 nm) band emission corresponds to the singly ionized oxygen vacancy and this emission results from the recombination of a photo-generated hole with the single ionized charge state of specific defects[26]. Fe-doped ZnO samples (Fig-5b) show that the V_O are also observed to be responsible for blue (458 nm) and green (510 and 535 nm) emissions. The V_O on the surface has been indicated to be the most likely candidate for recombination state. The weak blue emission around 458 nm can be represented to the energy transition of electron from Zn_i to V_{Zn}. The blue green emission of 488 nm is likely to surface defects in the ZnO nanocrystals. It can be attributed to the transition between V_O to O_i. The green emission also represents the transition of photogenrated electron from the C_B edge to a trap level. The green-yellow peak (573 nm) has represented the defect complex of V_OZn_i[27]. As the results indicate, the solution incineration process formed more visible emissions in the Ag as well as Fe-doped ZnO nanoparticles, which in turn improved the optical properties.

Conclusion:

The comparative study of Raman and PL studies of Ag and Fe-doped ZnO nanoparticles synthesized by simple solution combustion method was reported. The XRD pattern show that the ZnO samples are in hexagonal wurtzite structure and secondary phase are in FCC structures. The FE-SEM images show the particles surface morphology was in aggregated nature. The Raman spectra of the both Ag and Fe-doped ZnO nanoparticles confirms the significant effect on polar and non-polar modes, when it is compared with the pure ZnO nanoparticles. The results of Ag-doped ZnO nanoparticles have rapidly changed their higher frequency modes and breakdown of translational crystal symmetry; however Fe-doped ZnO nanoparticles are gradually changed and peaks are broadened as well as shifted to lower energy. The PL results are related to some fundamental defects such as V_O, V_{Zn}, O_i etc. in both Ag and Fe-doped ZnO nanoparticles, respectively. The Fe-doped ZnO nanoparticles show the blue shift of NBE emission into UV region due to Burstein-Moss effect. The results demonstrate that Raman and PL spectroscopy are essential diagnostic tools for determining the structural, vibrational and optical properties of Ag and Fe-doped ZnO nanoparticles.

References:

1. Özgür. Ü, Alivov. Y.I, Liu. C, Teke. A, Reshchikov. M.A, Doğan. S, Avrutin. V, Cho. S.-J and Morkoç. H, A comprehensive review of ZnO materials and devices, J. Appl. Phys. 2005, 98, 041301.
2. Cao. L, White. J.S, Park. J.S, Schuller J.A, Clemens B.M, Brongersma M.L, Engineering light absorption in semiconductor nanowire devices, Nat Mater. 2009, 8, 643-647.
3. Tankhiwale. R, Bajpai. S.K, Preparation, characterization and antibacterial applications of ZnO-nanoparticles coated polyethylene films for food packaging, Colloids Surf., B, 2012, 90, 16-20.
4. Wang. Z.L, Zinc oxide nanostructures: growth, properties and applications, J. Phys.: Condens. Matter, 2004, 16, R829.

5. Gomez. J. L and Tigli. O, Zinc oxide nanostructures: from growth to application, J. Mater. Sci. 2013, 48, 612-624.
6. Schmidt-Mende. L and MacManus-Driscoll. J.L, ZnO – nanostructures, defects, and devices, Mater. Today, 2007, 10, 40-48.
7. Purica. M, Budianu. E and Rusu. E, ZnO thin films on semiconductor substrate for large area photodetector applications, Thin Solid Films, 2001, 383, 284–286.
8. Zhang. J, He. M, Fu. N, Li. J and Yin. X, Facile one-step synthesis of highly branched ZnO nanostructures on titanium foil for flexible dye-sensitized solar cells, Nanoscale, 2014, 6, 4211-4216.
9. Krebs. F.C, Thomann. Y, Thomann. R and Andreasen. J.W, A simple nanostructured polymer/ZnO hybrid solar cell—preparation and operation in air, Nanotechnology, 2008, 19, 424013.
10. Chen. S, Shi. J, Kong. X, Wang. Z and Liu. D, Cavity coupling in a random laser formed by ZnO nanoparticles with gain materials, Laser Phys. Lett. 2013, 10, 055006.
11. J Pearton S.J, Norton. D.P, Ivill. M.P, Hebard. A.F, Chen. W.M, Buyanova. I.A and Zavada. J.M, Transition Metal Doped ZnO for Spintronics, MRS Proc. 2007, 999, K03-04.
12. Silambarasan. M, Saravanan. S and Soga. T, Mn-Doped ZnO Nanoparticles Prepared by Solution Combustion Method, e-J. Surf. Sci. Nanotech. 2014, 12, 283-288.
13. Djurišić Dr. A.B and Leung. Y.H, Optical Properties of ZnO Nanostructures, 2006, 2, 944–961.
14. Sato-Berrú. R.Y, Vázquez-Olmos A, Fernández-Osorio. A.L and Sotres-Martínez. S, Micro-Raman investigation of transition-metal-doped ZnO nanoparticles, J. Raman Spectrosc. 2007, 38, 1073-1076.
15. Pál. E and Dékány. I, Structural, optical and photoelectric properties of indium-doped zinc oxide nanoparticles prepared in dimethyl sulphoxide, Colloids Surf., A, 2008, 318, 141–150.
16. Wu. L, Wu. Y, Pan. X and Kong. F, Synthesis of ZnO nanorod and the annealing effect on its photoluminescence property, Opt. Mater., 2006, 28, 418–422.
17. Wu. L, Wu. Y and LÜ. W, Preparation of ZnO nanorods and optical characterizations, Physica E:, 2005, 28, 76–82.
18. Silambarasan. M, Saravanan. S, Ohtani. N and Soga. T, Structural and optical studies of pure and Ni-doped ZnO nanoparticles synthesized by simple solution combustion method, Jpn. J. Appl. Phys. 2014, 53, 05FB16.
19. Saravanan. S, Silambarasan. M and Soga. T, Structural, morphological and optical studies of Ag-doped ZnO nanoparticles synthesized by simple solution combustion method, Jpn. J. Appl. Phys. 2014, 53, 11RF01.
20. Hou. Y, Xu. Z and Sun. S, Controlled Synthesis and Chemical Conversions of FeO Nanoparticles, Angew. Chem. Int. Ed., 2007, 46, 6329-6332.
21. Wang. J.B, Huang G.J, Zhong X.L, Sun. L.Z, Zhou. Y.C and Liu. E.H, Raman scattering and high temperature ferromagnetism of Mn-doped ZnO nanoparticles, Appl. Phys. Lett. 2006, 88, 252502.
22. Xu. C.X, Sun. X.W, Zhang. X.H, Ke. L and Chua. S.J, Photoluminescent properties of copper-doped zinc oxide nanowires, Nanotechnology, 2004, 15, 856.
23. Kim. K.J and Park. Y.R, Large and abrupt optical band gap variation in In-doped ZnO, Appl. Phys. Lett., 2001 78, 475.
24. Zeferino. R.S, Flores M.B and Pal. U. Photoluminescence and Raman Scattering in Ag-doped ZnO Nanoparticles, J. Appl. Phys. 2011, 109, 014308.
25. Stanković. A, Stojanović. Z, Veselinović. L, Škapin. S.D, Bračko. I, Marković. S and Uskoković. D, Mater. Sci. Eng., B, 2012, 177, 1038–1045.
26. Sabri. N.S, Yahya. A.K and Talari. M.K, Emission properties of Mn doped ZnO nanoparticles prepared by mechanochemical processing, J. Lumin., 2012, 132, 1735–1739.
27. Kumar. S, Mukherjee. S, Singh. R.Kr, Chatterjee. S and Ghosh. A.K, Structural and optical properties of sol-gel derived nanocrystalline Fe-doped ZnO, J. Appl. Phys., 2011, 110, 103508.

*****